

# Hydrophobicity and Adhesion of Aggregated Diamond Particles

Kaili Yao, Bing Dai,\* Paul W. May, Xiaojun Tan, Jiecai Han, and Jiaqi Zhu\*

Diamond powders with high hydrophobicity are prepared by etching graphite plates using a hydrogen/argon ( $H_2/Ar$ ) plasma. The morphology and size of the diamond powders are found to vary with the proportion of Ar in  $H_2$  from 0% to 50%. Wettability is measured using water contact angle (WCA) measurements giving values between  $129.7^\circ$  and  $146.9^\circ$ . The high hydrophobicity can be ascribed to the aggregated structure of the as-grown diamond powders. To check this assumption, the aggregated diamond powders are separated into individual particles by mechanical grinding; then, the WCAs of separated as-grown diamond powders and commercial dispersed diamond powders are compared. The separated diamond surfaces show the lower WCAs of  $99.68^\circ$  and  $96.96^\circ$ . The surface of the aggregated diamond powders also exhibits high adhesion to water. The diamond surface grown in 2% Ar suspends  $40\ \mu\text{L}$  of water under a tilt angle of  $180^\circ$ . Such aggregated diamond powders are promising for no-loss liquid transportation.

that the polymer fabrication procedures are often complicated and involve several steps, are currently impediments to the usage of these materials for real-world applications.

Diamond exhibits a series of extraordinary properties, such as extreme mechanical hardness, high chemical stability, and high resistance to acids and alkalis.<sup>[5–7]</sup> The rapid advances in high-pressure high-temperature (HPHT) and chemical vapor deposition (CVD) of diamond over the last decade<sup>[8,9]</sup> now mean that diamond in various forms (single-crystal gemstones, thin layers, or powders) can be purchased from a wide range of commercial suppliers at inexpensive prices. As such, diamond is becoming a promising material for a range of engineering applications, including those which require a controlled hydrophobic or hydrophilic surface, especially in

## 1. Introduction

Materials with high hydrophobicity and adhesion performance toward water are increasingly in demand by industry.<sup>[1]</sup> These materials have attracted much interest in the area of self-cleaning, programmed liquid transportation, microfluidic devices, vapor condensation, and microelectromechanical system building.<sup>[2,3]</sup> Most scientific reports about such materials describe their fabrication using modified or functionalized polymers, such as polytetrafluoroethylene or octadecylamine.<sup>[4]</sup> However, such functionalized polymerized materials have some limitations, including poor abrasive resistance, chemically instability, and low lifetime. These issues, combined with the problem

extreme environments. Therefore, understanding what determines the wettability (hydrophilicity) of diamond is crucial if these surface properties are to be reliably tailored to a particular application.

The standard test for wettability is to measure the contact angle made by a water droplet placed onto the surface.<sup>[10,11]</sup> A water contact angle (WCA) of  $<90^\circ$  means the droplet spreads on the surface, so the surface is hydrophilic. Complete wetting is when the  $WCA = 0^\circ$ , and the droplet forms a flat liquid layer on the surface. In contrast,  $WCA > 90^\circ$  means the water droplet is being repelled from the surface; i.e., the surface is hydrophobic. Samples where the WCA is  $\gg 90^\circ$  mean that the water droplet remains nearly spherical, with minimal contact with the surface—in this case, the surface is said to be superhydrophobic.


The WCA of single crystalline diamond is  $\approx 93^\circ$ <sup>[11,12]</sup>; i.e., it is reasonably hydrophilic; however, this value depends greatly upon the surface termination and its morphology.<sup>[13,14]</sup> Different chemical species terminating a diamond surface may either attract or repel water molecules, influencing both the surface hydrophilicity and adhesion properties. For example, an oxidized diamond surface is very hydrophilic, whereas a hydrogenated surface is hydrophobic. Aminated ( $-NH_2$ ) diamond surfaces are slightly hydrophobic, whereas fluorinated ones can be superhydrophobic.<sup>[15]</sup>

Diamond surface morphology also affects wettability. For example, Ostrovskaya et al. grew ultrananocrystalline diamond (UNCD) films on silicon substrates in a microwave plasma CVD system.<sup>[7,11]</sup> The UNCD films exhibited a higher WCA of  $124^\circ$  compared with that of a smooth single-crystalline diamond. This was ascribed to the high nanoporosity and passivated

K. Yao, Dr. B. Dai, X. Tan, Prof. J. Han, Prof. J. Zhu  
Center for Composite Materials and Structures  
Harbin Institute of Technology  
Harbin 150080, P. R. China  
E-mail: daib@hit.edu.cn, daibinghit@vip.126.com; zhujuq@hit.edu.cn

K. Yao, Prof. P. W. May  
School of Chemistry  
University of Bristol  
Cantock's Close, Bristol BS8 1TS, UK

Prof. J. Zhu  
Key Laboratory of Micro-systems and Micro-structures Manufacturing,  
Ministry of Education  
Harbin Institute of Technology  
Harbin 150080, P. R. China

 The ORCID identification number(s) for the author(s) of this article can be found under <https://doi.org/10.1002/pssa.202000355>.

DOI: 10.1002/pssa.202000355

surface of the UNCD film. Wang et al. also prepared porous diamond films, which, after hydrogen etching, showed a WCA of  $138.5^\circ$ .<sup>[13]</sup> Dunseath et al. fabricated diamond-coated nanoneedles, which exhibited large differences in WCA from the flat diamond control samples.<sup>[15]</sup> These differences were ascribed to the increased surface area of the nanoneedles, amplifying the water/surface interactions.

As well as the wettability, a related property of interest is droplet adhesion, which is a measure of the droplet's propensity to move around the surface when it is tilted or disturbed. Although water droplets will form on all hydrophobic surfaces, their adhesion behavior may be very different depending upon the chemical interactions involved and the surface structure. Two surfaces with similar (super)hydrophobicities may exhibit very different adhesion behaviors, because their surfaces are textured with different length scales of roughness. For example, many surfaces (especially those in nature, such as leaves) contain microscale structures (e.g., folds and wrinkles) that are themselves covered in nanoscale structures (e.g., spikes and hairs). The nanoscale structures make the overall surface net-hydrophobic, but the size of the microstructures determines whether water can permeate in between them to interact with the entire surface. On larger scale microstructures, where water permeation is possible, the adhesion forces are increased, and the spherical water drops tend to remain immobile. This homogeneous wetting is sometimes called the "petal effect"<sup>[16–18]</sup> and was modeled by Marmur and Wenzel.<sup>[19–21]</sup> Conversely, on smaller scale microstructures where water permeation cannot occur, air gaps are created at the interface, greatly reducing adhesion, and the water droplets easily roll away. This is called the "lotus leaf effect"<sup>[22]</sup> and was modeled by Whyman and Cassie and Baxter.<sup>[23,24]</sup>

Adhesion of water to surfaces can be measured by several ways. Ding et al.<sup>[1,4]</sup> measured the adhesive performance of surfaces by placing water droplets onto the sample surface while gradually inclining it using a tilting platform. The larger the tilt angle before the drop rolled off, the higher the adhesive force. Jin et al. measured the adhesive behavior via a microelectromechanical balance system.<sup>[25]</sup> A water drop was suspended with a fixed metal cap. The stage was moved upward at a constant speed until its surface contacted the droplet. Then, the stage was moved down; the point when the surface just broke away from the water droplet determined the adhesive force. Although this method can measure a specific value of adhesive force for the tested material, it requires an expensive microelectromechanical balance system and careful observation. In contrast, Li et al. assessed the adhesion by turning the sample surface supporting a water droplet upside down, and measuring the maximum volume of water droplet that remained stuck to the sample surface.<sup>[26]</sup> This measurement method is straightforward and reliable and was the method of choice adopted in our study. This was because the relative difference in adhesion behavior for different samples could be assessed simply by comparing the volume of water drops suspended in each case.

Being able to independently control the hydrophobicity and adhesion of water droplets on a surface allows a great deal of flexibility in the design of smart materials. Such multifunctional superhydrophobic surfaces can satisfy multiple requirements, such as those found in sensors, microdroplet manipulation, and wearable devices.

One of the very few related studies concerning the adhesive force of water on diamond is from Wang et al. who reported diamond microspheres, which exhibited superhydrophobic properties in the pH range of 1–14.<sup>[27]</sup> The diamond nanospheres prevented a  $5\ \mu\text{L}$  water droplet from falling off when the tilt angle was  $180^\circ$ .

In this study, we investigated the water wettability and the adhesion forces of as-grown aggregated diamond powders, and the results compared with those from diamond films and aggregated diamond powders.

## 2. Results and Discussion

The SEM images of diamond powders grown with 0%, 2%, 5%, 10%, 20%, and 50% Ar in  $\text{H}_2/\text{Ar}$  gas mixture are shown in **Figure 1a–f**. The diamond particles are near spherical and aggregated into clusters as a result of continuous re-nucleation during diamond growth.<sup>[5]</sup> The aggregated clusters increase the roughness and surface area.<sup>[21,27,28]</sup> The surface morphologies of the aggregates change with increasing Ar flow rates, as shown in **Figure 1** and **2**.

**Figure 2** shows that the diamond grain sizes become smaller with the increase in the Ar: $\text{H}_2$  ratio in the gas mixture. In a pure  $\text{H}_2$  atmosphere (**Figure 2a**), the crystallites are large ( $4\text{--}5\ \mu\text{m}$ ), well faceted, and exhibit mainly a (111) crystal orientation. There is a decrease in crystallite size to  $\approx 2\ \mu\text{m}$  when the diamond powders are grown in 2% Ar in  $\text{Ar}/\text{H}_2$  (**Figure 2b**), but the facets seem slightly better defined. With further increases in Ar flow rate (**Figure 2c–f**), the (111) orientation gradually disappears, whereas nanodiamond morphologies emerge instead. For powders grown with 50% Ar (**Figure 2f**), the crystallite size decreased to  $\approx 100\ \text{nm}$ , although the overall cluster morphology retains a spherical template. The key point from these images is that all the powders exhibited nanoscale structures superimposed upon microscale structures, and so are potential candidates to have overall hydrophobic surfaces but with differing adhesion properties.

**Figure 3** shows the laser Raman spectra of the various diamond powders. Every curve shows a clear  $\text{sp}^3$  diamond peak at  $\approx 1332\ \text{cm}^{-1}$ . The spectrum from the sample grown with 2% Ar has the sharpest  $\text{sp}^3$  carbon peak of all curves, consistent with the well-defined facets shown in **Figure 2b**. The peak intensity then decreases with increasing Ar proportion from 5% to 50%, whereas the broad features consistent with the  $\text{sp}^2$  carbon D and G bands start to emerge in the range of  $1350\text{--}1600\ \text{cm}^{-1}$ . These observations are both consistent with the crystallite size shrinking while the number of grain boundaries increases. When the ratio of Ar reached 50%, a feature at  $\approx 1130\ \text{cm}^{-1}$  emerged, which has been attributed to  $\text{sp}^2$  carbon species, such as *trans*-polyacetylene, present in grain boundaries and is an indicator of nanocrystalline diamond.<sup>[29,30]</sup> A more detailed analysis of the Raman spectra can be found in the Supporting Information.

The XRD patterns of samples grown with 0%, 2%, 10%, and 50% Ar are presented in **Figure 4**. There are four main peaks in the spectra:  $43.8^\circ$ ,  $75.2^\circ$ ,  $91.2^\circ$ , and  $119.3^\circ$ , corresponding to (111), (220), (311), and (400) diamond crystal planes, respectively. In addition, the curves become noisier with increasing Ar

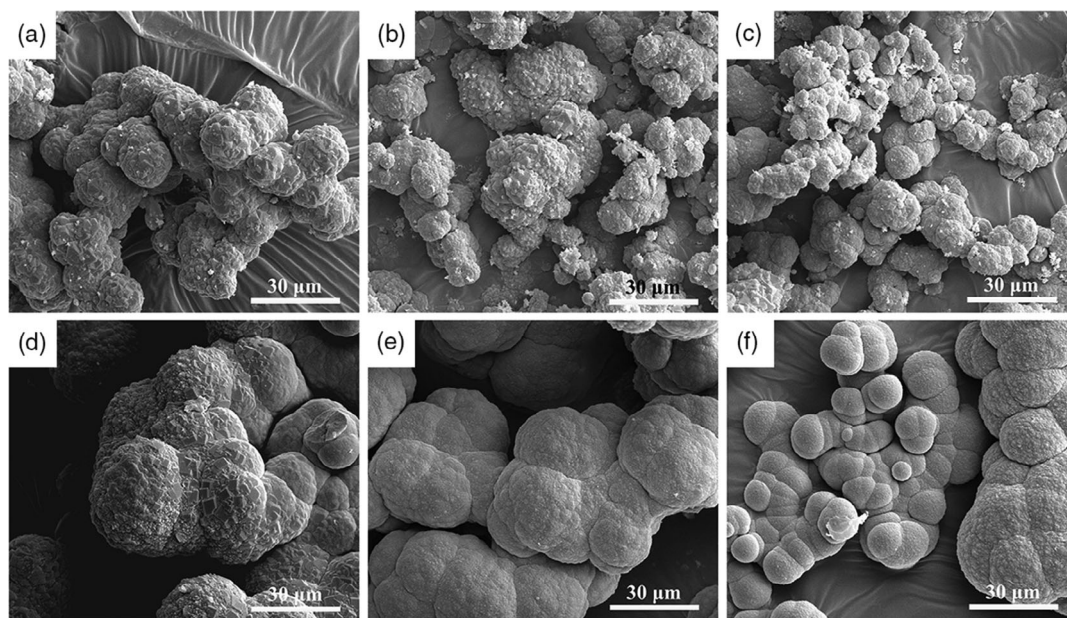


**Figure 1.** SEM images for the aggregated diamond powders grown with a–f) 0%, 2%, 5%, 10%, 20%, and 50% Ar during plasma etching of graphite plates, respectively.

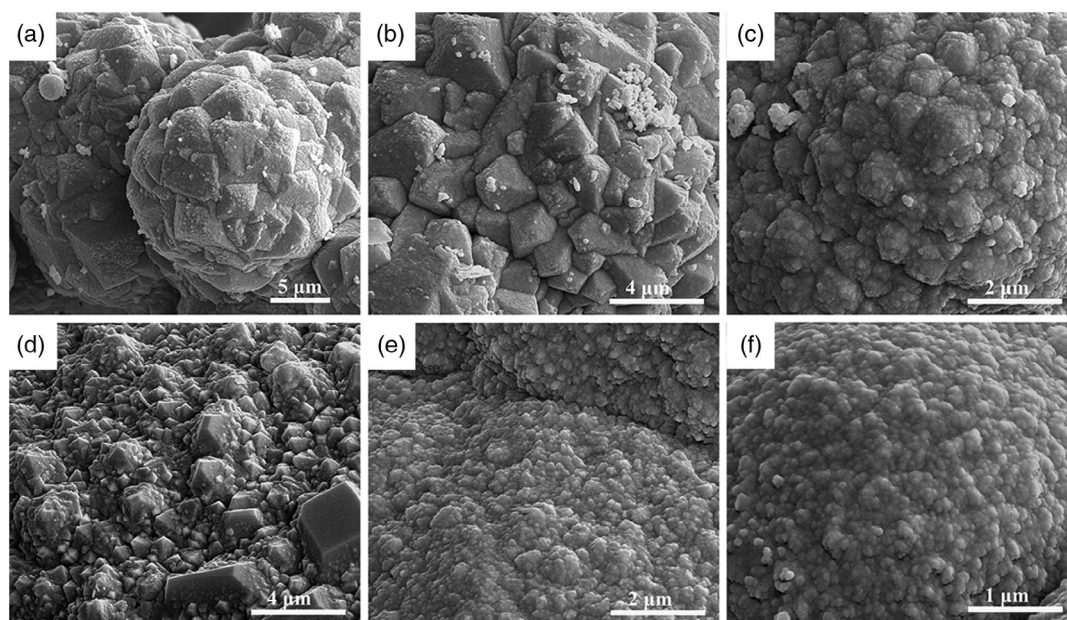


**Figure 2.** Higher-magnification SEM images of the diamond particles grown with the same conditions as in Figure 1.

proportion, which can be ascribed to the decreasing diamond grain sizes (as shown in Figure 2), which will weaken the X-ray signal. The average crystallite sizes of the diamond grown from 0%, 2%, 5%, 10%, 20%, and 50% derived from the XRD patterns are 161.3, 146.9, 102.5, 63.0, 24.4, and 23.6 nm, respectively.

The WCA values of diamond powders grown with 0%, 2%, 5%, 10%, 20%, and 50% Ar in Ar/H<sub>2</sub> were tested and found to be 140.1°, 146.9°, 144.8°, 129.7°, 137.0°, and 138.7°,

respectively. The WCA of the uncoated double-sided tape was also tested (see Supporting Information) and found to be <90°. This suggests that the underlying double-sided tape is not affecting the WCA values for the diamond particles, and that the WCA values are representative of the diamond powder.

The diamond powders grown with 2% Ar were the most hydrophobic of those tested. **Figure 5** shows a representative optical photograph of the water-droplet shapes on the diamond powders grown with 2% Ar in Ar/H<sub>2</sub>. Optical photographs of those

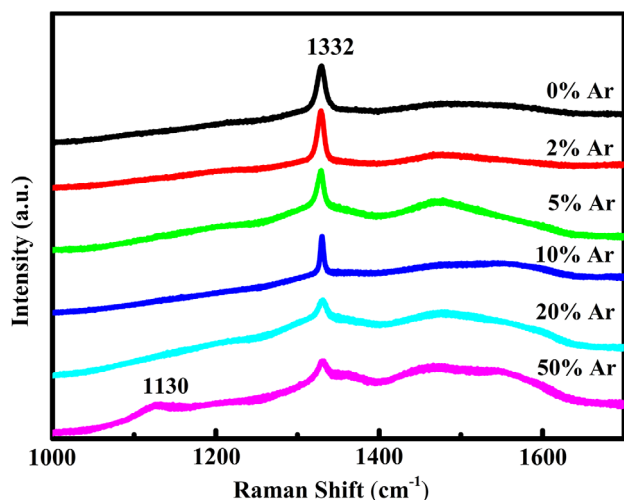


**Figure 3.** Raman spectra of diamond particles grown with 0%, 2%, 5%, 10%, 20%, and 50% Ar during plasma etching of graphite plates.

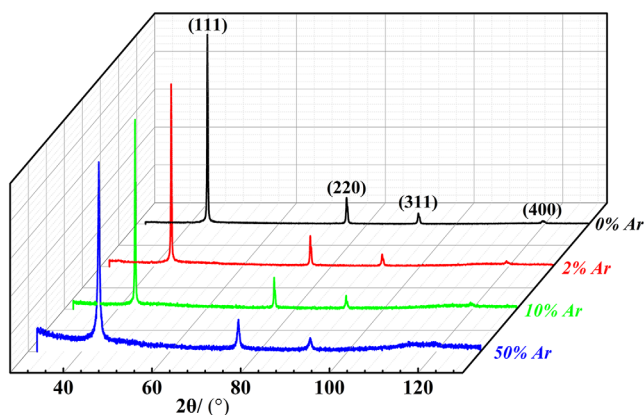


**Figure 4.** Normalized XRD patterns of the diamond samples grown using 0%, 2%, 10%, and 50% Ar in H<sub>2</sub>.

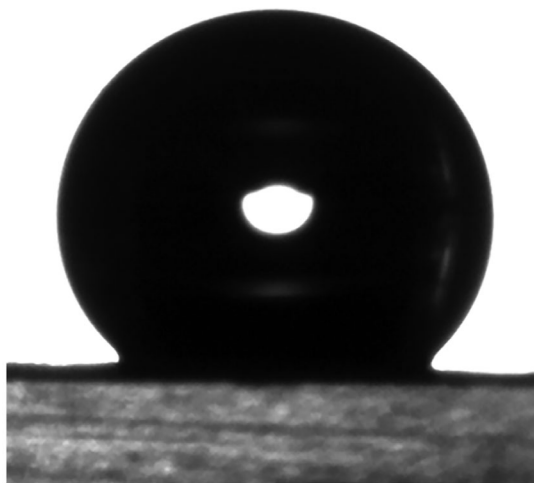


**Figure 5.** Optical photograph for the water droplets on the diamond powder grown with 2% Ar in H<sub>2</sub>.

samples grown with 0%, 5%, 10%, 20%, and 50% Ar in Ar/H<sub>2</sub> can be found in the Supporting Information. Compared with the WCA results of diamond films mentioned in Section 1, the WCA value of diamond powders grown with 2% Ar shows larger values than either single-crystal diamond (93°) or nanocrystal diamond films (124°).<sup>[7,11]</sup> The hydrophobic properties of the as-grown diamond powders are partly due to their aggregation and mixed micro-/nanoscale structure,<sup>[27]</sup> as well as to their hydrogen termination.

For comparison, the as-grown aggregated diamond powders were separated into individual particles by mechanical grinding for 30 min in a stainless-steel mortar.<sup>[5]</sup> SEM images of the deaggregated diamond particles are shown in Figure 6a. The particles were attached to a glass slide as described earlier and the WCA measured. The analysis of the image shown in Figure 6b determined the WCA of the mechanically separated diamond particles to be ≈99.68°.

In addition, we also compared the WCA of 20 μm commercial diamond powders purchased from Zhengzhou Sino-Crystal Diamond Company. The SEM image and optical photographs of the water droplets on these purchased diamond powders are given in Figure 6c,d. The analysis of the image shown in Figure 6d determined the WCA of the commercial diamond particles to be ≈96.96°.

For adhesion measurements, the samples generated with 2% and 50% Ar/H<sub>2</sub> were tested using different sizes of water droplet. As shown in Figure 7a,b, a 10 μL water droplet did not fall off the diamond surface even after it was tilted through 90° or 180°. Larger water droplets with the volumes of 15 and 20 μL also did not fall off under a tilt angle of 180°, as shown in Figure 7c,d. When the water droplet volume reached 23 μL, the water droplet fell off (Figure 7e). These tests were repeated with the other diamond powders. It was found that the powder grown with 2% Ar/H<sub>2</sub> had the best adhesion ability of all the samples tested, and was able to retain a 40 μL water droplet on its surface at 180°. The high hydrophobicity and adhesion behavior are consistent with the Wenzel model of adhesion.<sup>[20,21,31]</sup> This model assumes that the liquid droplet has complete contact with a surface, and is used to describe the situation in which droplets penetrate any rough structures leading to high adhesive forces. The aggregated diamond powder surface is rough on the nanoscale, which increases the hydrophobicity resulting in high WCA. However, the surface of the powder layer has a relatively large microstructure, being composed of micrometer-sized particles. Hence, water may permeate between the particles on the sample surfaces generating strong adhesion forces.

### 3. Conclusion

In summary, diamond powders with low wettability (high hydrophobicity) were produced via microwave plasma etching of graphite plates using a hydrogen and argon gas mixture. The morphology of the resulting diamond powders varied in microstructure depending on the Ar/H<sub>2</sub> mixing ratio. With little or no Ar addition, the mainly H<sub>2</sub> atmosphere produced diamond powder with well-defined, micro-scale faceted crystallites.<sup>[32]</sup> This is consistent with what is known<sup>[33,34]</sup> about the mechanisms for the growth of diamond via CVD, which relies on a high ratio

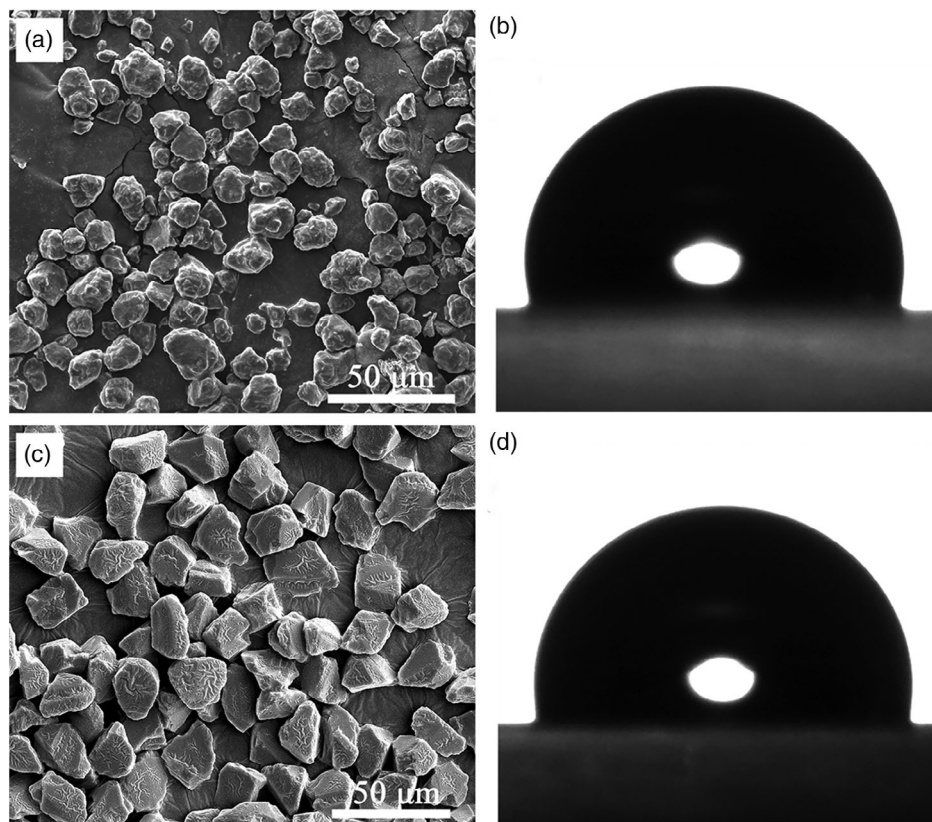


**Figure 6.** SEM images and optical photographs of the water droplets from a,b) individual diamond particles made by grinding the grown aggregated diamond powders and c,d) commercial separated diamond particles.

of H atoms to carbon radical species ( $H: C_xH_y$ ) near the surface to deposit  $sp^3$  diamond rather than  $sp^2$  graphitic carbon. In our CVD system, the graphite disks act as the carbon source, which is etched by H atoms to form the gas-phase  $CH_3$  radicals responsible for diamond growth. With proportionately more Ar added to the gas mixture, the H atom concentration falls, and thus, the  $CH_3$  species now react to form larger reactive hydrocarbons ( $C_xH_y$ ), which are believed to play a role in the growth of non-diamond phases. This results in more  $sp^2$  carbon becoming incorporated into the growing diamond powders, reducing the crystallite size, and increasing the number of grain boundaries, as evidenced in the corresponding XRD, Raman, and SEM images. Thus, the growth mechanism in our system appears to be consistent with that seen in standard CVD systems. The observation that the best (i.e., highest  $sp^3$  carbon content) powders were produced at 2% Ar/ $H_2$  is probably due to the small Ar addition stabilizing the plasma by electron injection, thereby increasing the dissociation of  $H_2$  into H. However, these benefits are negated at >2% addition of Ar by the increasing dilution of the chemically active  $H_2$  gas by inert Ar. Another consequence of Ar addition is an increase in the concentration of  $Ar^+$  ions in the plasma, which increase the plasma potential, and, thus, the potential difference between the plasma and the grounded substrate. As a result, both the intensity and kinetic energy of  $Ar^+$  ion impacts upon the growing surface increase, which damage the diamond lattice and initiate secondary nucleation processes.

Consequently, as Ar concentrations approach 50%, the crystallite size rapidly decreases.

The WCAs of the as-grown diamond powders were all  $130^\circ$ – $147^\circ$ , making them all hydrophobic. This is consistent with these powders having an H termination, a large surface area, and a mixture of nanoscale and microscale morphology.

The purchased microdiamond powders and our synthesized and then separated diamond powders show the similar WCA values of  $96^\circ$ – $99^\circ$ , which is lower than the as-grown aggregated diamond powders. This is probably due to the lower surface nanoscale roughness of the purchased and separated powders. The purchased powders are composed of  $20\ \mu m$  diamond, which has relatively smooth surfaces and facets, with little nanostructure (see Figure 6b). The deaggregated powder has had most of the delicate nanostructures polished away during the milling process, leaving mainly micrometer-sized particles (Figure 6a).

The surface of the aggregated diamond powders exhibited a high adhesion to water, being able to hold a  $40\ \mu L$  water droplet at a tilt angle of  $180^\circ$ . For comparison, Wang et al.<sup>[27]</sup> reported that composite diamond microspheres could keep  $5\ \mu L$  water droplets stable at  $180^\circ$ , whereas Li et al.<sup>[26]</sup> developed a novel superhydrophobic cerium dioxide nanotube material, which retained  $20\ \mu L$  water droplets. Our aggregated diamond powders show better adhesive ability to water than either of these reports, and so are promising for liquid-transfer applications. The study of water adhesion on diamond powders is a novel area of

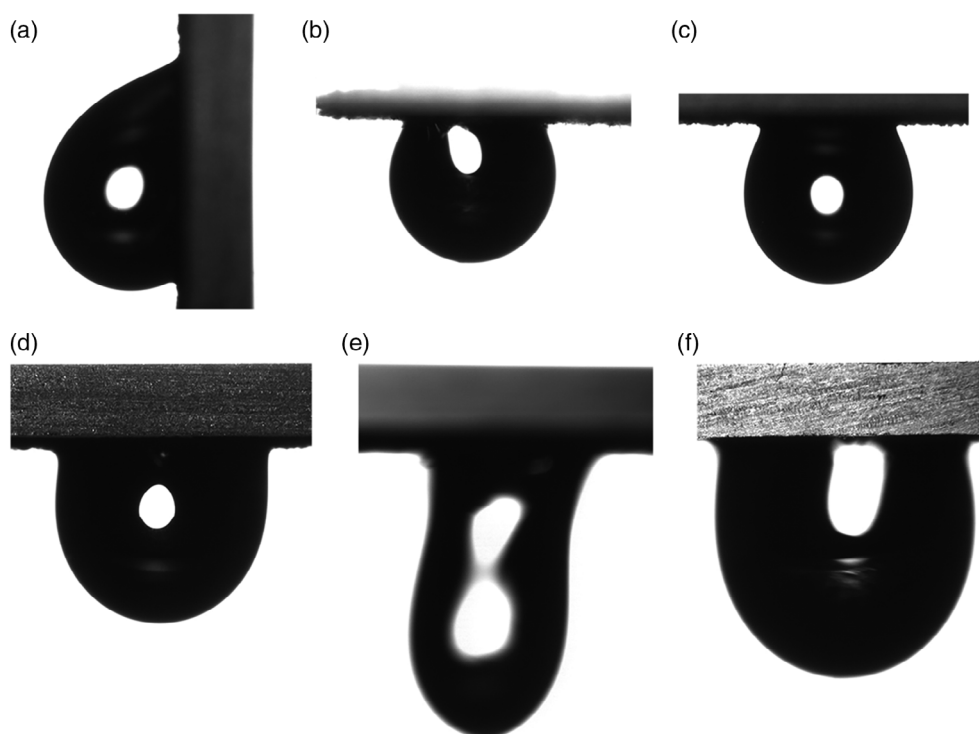


**Figure 7.** a–e) Optical photographs for water droplets of different volumes on the diamond grown with 50% Ar/H<sub>2</sub>. The behavior of the diamond grown with 2% Ar/H<sub>2</sub> was almost identical to the 50% Ar/H<sub>2</sub> sample, except with slightly higher values for droplet volume in each case due to its improved adhesion. f) Thus, only the 180° tilt angle image is shown for this sample. The photographs are: diamond grown with 50% Ar/H<sub>2</sub> with a) 10 µL under a tilt angle of 90°, and then under a tilt angle of 180° with droplet volumes of b) 10 µL, c) 15 µL, d) 20 µL, and e) 23 µL. f) 40 µL water droplet on the diamond grown with 2% Ar under a tilt angle of 180°.

research, and only a few preliminary results are presented here. However, this field has great potential for future detailed study.

#### 4. Experimental Section

Aggregated diamond powders were grown using a microwave plasma CVD reactor.<sup>[32]</sup> The gas mixture consisted of hydrogen and argon (both 99.999%) with a total gas flow rate of 200 sccm. Diamond powders with different properties were made by varying the Ar flow rate as follows: 0, 4, 10, 20, 40, and 100 sccm, equivalent to 0%, 2%, 5%, 10%, 20%, and 50% of the total flow rate. The carbon source was a graphite plate of diameter 50 mm and thickness 2 mm, which was positioned on the substrate holder and acted as the substrate for holding the grown aggregated diamond powders.<sup>[5,6]</sup> Samples were grown at a pressure and an MW power of 128 mbar and 2800 W, respectively, for a growth time of 10 h. The substrate temperature was 750–800 °C, measured by a Williamson PRO 92-40-C pyrometer.<sup>[35]</sup> After growth, the as-grown diamond powders lay loosely on the surface of the graphite plate and were collected by inclining the graphite plates and sweeping the powder into a plastic tray. A detailed description of the apparatus and process can be found elsewhere.<sup>[5]</sup>

The morphologies of the aggregated diamond powders were imaged by a field-emission scanning electron microscopy (FE-SEM) (Helios Nanolab 600i). Laser Raman spectroscopy (HORIBA LabRAM HR Evolution, 532 nm excitation) and X-ray diffraction (XRD; PANalytical X'Pert Pro MPD) were used to measure the phase purity and orientations of diamond powders. Analysis of the XRD patterns to determine the crystallite size of the diamond samples was performed using Jade Software (MDI JADE 6 Materials Data XRD Pattern Processing, Identification, and Quantification).

The WCA was measured via water droplet analysis (Theta Lite, Biolin) with the volume of water droplet fixed at 10 µL. For the WCA analysis, the aggregated diamond powders were stuck onto a glass slide using double-sided tape (DELI Ltd., Cat. No. 30400). First, the tape was attached to the surface of the glass, and excess diamond powder was dropped onto this tape. Any diamond powder that did not adhere to the tape was removed by shaking to ensure there were no gaps in the continuous diamond layer. The outward-facing side of the diamond powder, which did not touch the tape, was used to measure the WCA. Photographs of the double-sided tape on the glass slide, both uncoated and coated with diamond powder, are shown in the Supporting Information. WCA values presented here are the average of three measurements and analyzed by *OneAttention* software. In addition, 3D topographies were taken with a USB 3.0 digital camera. Ambient humidity and temperature are not believed to be major factors in WCA measurements; nevertheless, we ensured that the WCA measurements for our samples were all taken over a period of only a few hours on the same day, so that the humidity and temperature would have remained almost constant.

The water adhesion properties of the aggregated diamond powders were tested by adding water droplets with varying volumes to the surface of the powder on a glass slide (prepared in the same way as for the WCA tests), and then tilting the glass slide through various angles under gravity, from 0° (horizontal), 90° (vertical), and 180° (inverted), and seeing if the droplet remained stuck to the surface or fell off.

For comparison, our as-grown aggregated diamond powders were separated into individual particles by mechanical grinding for 30 min in a stainless-steel mortar.<sup>[5]</sup> In addition, we purchased 20 µm commercial diamond powders from Zhengzhou Sino-Crystal Diamond Company. These two types of powders were tested for WCA and compared with our aggregated samples.

## Supporting Information

Supporting Information is available from the Wiley Online Library or from the author.

## Acknowledgements

This work was supported by the National Natural Science Foundation of China (Grant No. 51702066), the National Key Research and Development Program of China (Grant No. 2016YFE0201600), the National Science Fund for Distinguished Young Scholars (Grant No. 51625201), International Science & Technology Cooperation Program of China (Grant No. 2015DFR50300), Key Laboratory of Micro-systems and Micro-structures Manufacturing, Ministry of Education, Harbin Institute of Technology (Grant No. 2016KM001), 1000 talents program, Innovative research group of NSFC 11421091, and China Scholarship Council.

## Conflict of Interest

The authors declare no conflict of interest.

## Keywords

adhesive force, aggregated diamond powders, etching, graphite, hydrophobicity

Received: June 11, 2020

Revised: October 7, 2020

Published online: November 4, 2020

- [1] G. Ding, W. Jiao, R. Wang, Z. Chu, Y. Huang, *J. Mater. Chem. A* **2019**, *7*, 12333.
- [2] G. Ding, W. Jiao, R. Wang, M. Yan, Z. Chu, X. He, *J. Mater. Chem. A* **2019**, *7*, 17766.
- [3] X.-P. Li, Y.-L. Sun, Y.-Y. Xu, Z.-S. Chao, *Small* **2018**, *14*, 1801040.
- [4] G. Ding, W. Jiao, L. Chen, M. Yan, L. Hao, R. Wang, *J. Mater. Chem. A* **2018**, *6*, 16992.
- [5] K. Yao, B. Dai, J. Zhu, V. Ralchenko, G. Shu, J. Zhao, P. Wang, B. Liu, G. Gao, M. Sun, K. Liu, Z. Lv, L. Yang, J. Han, *Powder Technol.* **2017**, *322*, 124.
- [6] K. Yao, B. Dai, V. Ralchenko, G. Shu, J. Zhao, K. Liu, Z. Yang, L. Yang, J. Han, J. Zhu, *Diam. Relat. Mater.* **2018**, *82*, 33.
- [7] L. Ostrovskaya, V. Perevertailo, V. Ralchenko, A. Saveliev, V. Zhuravlev, *Diam. Relat. Mater.* **2007**, *16*, 2109.
- [8] M. Schwander, K. Partes, *Diam. Relat. Mater.* **2011**, *20*, 1287.
- [9] S. Eaton-Magaña, J. E. Shigley, C. M. Breeding, *Gems Gemo.* **2017**, *53*, 262.
- [10] D. Y. Kwok, A. W. Neumann, *Adv. Colloid Interface Sci.* **1999**, *81*, 167.
- [11] L. Y. Ostrovskaya, V. G. Ral'chenko, I. I. Vlasov, A. A. Khomich, A. P. Bol'shakov, *Prot. Met. Phys. Chem.* **2013**, *49*, 325.
- [12] J. Hansen, R. Copperthwaite, T. Derry, J. Pratt, *J. Colloid Interface Sci.* **1989**, *130*, 347.
- [13] Q. Wang, J. Bai, B. Dai, L. Yang, P. Wang, Z. Yang, S. Guo, Y. Zhang, J. Han, J. Zhu, *Carbon* **2018**, *129*, 367.
- [14] Y. B. Zhou, Y. Yang, W. M. Liu, Q. Ye, B. He, Y. S. Zou, P. F. Wang, X. J. Pan, W. J. Zhang, I. Bello, S. T. Lee, *Appl. Phys. Lett.* **2010**, *97*, 133110.
- [15] O. Dunseath, E. J. W. Smith, T. Al-Jeda, J. A. Smith, S. King, P. W. May, A. H. Nobbs, G. Hazell, C. C. Welch, B. Su, *Sci. Rep.* **2019**, *9*, 8815.
- [16] G. Ding, W. Jiao, R. Wang, Y. Niu, L. Hao, F. Yang, W. Liu, *J. Mater. Chem. A* **2017**, *5*, 17325.
- [17] H. Zhu, Z. Guo, W. Liu, *Chem. Commun.* **2014**, *50*, 3900.
- [18] L. Feng, Y. Zhang, J. Xi, Y. Zhu, N. Wang, F. Xia, L. Jiang, *Langmuir* **2008**, *24*, 4114.
- [19] A. Marmur, *Langmuir* **2003**, *19*, 8343.
- [20] R. N. Wenzel, *Ind. Eng. Chem.* **1936**, *28*, 988.
- [21] R. N. Wenzel, *J. Phys. Chem.* **1949**, *53*, 1466.
- [22] A. Lafuma, D. Quéré, *Nat. Mater.* **2003**, *2*, 457.
- [23] G. Whyman, E. Bormashenko, T. Stein, *Chem. Phys. Lett.* **2008**, *450*, 355.
- [24] A. Cassie, S. Baxter, *Trans. Faraday Soc.* **1944**, *40*, 546.
- [25] M. Jin, X. Feng, L. Feng, T. Sun, J. Zhai, T. Li, L. Jiang, *Adv. Mater.* **2005**, *17*, 1977.
- [26] X. P. Li, Y. L. Sun, Y. Y. Xu, Z. S. Chao, *Small* **2018**, *14*, e1801040.
- [27] Q. Wang, J. Bai, B. Dai, Z. Yang, S. Guo, L. Yang, Y. He, J. Han, J. Zhu, *Chem. Commun.* **2017**, *53*, 2355.
- [28] F. Pinzari, P. Ascarelli, E. Cappelli, G. Mattei, R. Giorgi, *Diam. Relat. Mater.* **2001**, *10*, 781.
- [29] A. C. Ferrari, J. Robertson, *Phys. Rev. B* **2001**, *63*, 121405.
- [30] R. Pfeiffer, H. Kuzmany, P. Knoll, S. Bokova, N. Salk, B. Günther, *Diam. Relat. Mater.* **2003**, *12*, 268.
- [31] M. Nosonovsky, *Langmuir* **2007**, *23*, 9919.
- [32] K. Yao, B. Dai, X. Tan, L. Yang, J. Zhao, V. Ralchenko, G. Shu, K. Liu, J. Han, J. Zhu, *CrystEngComm* **2019**, *21*, 2502.
- [33] S. J. Harris, *Appl. Phys. Lett.* **1990**, *56*, 2298.
- [34] F. Celii, D. White Jr, A. Purdes, *Thin Solid Films* **1992**, *212*, 140.
- [35] K. Yao, X. Tan, B. Dai, J. Bai, Q. Sun, W. Cao, J. Zhao, L. Yang, J. Han, J. Zhu, *J. Mater. Sci. Technol.* **2020**, *49*, 42.